2024 IEEE/RSJ International Conference on Intelligent Robots and Systems (IROS)
October 14-18, 2024. Abu Dhabi, UAE

Fingertip Tactile Sensor for Detecting Rope Slip

Takayuki Koga[1], Junya Sato[2], Takuya Daigo[2], Kohei Kimura[1] and Shunsuke Kudoh[1]

Abstract— **When a robot manipulates a flexible object, a delicate grasp is required. Slip is an important indicator that can enable a robotic manipulator to delicately grasp an object. Therefore, we created a 3×3 tactile sensor matrix covered with a elastomer grip, intended to be used on a robotic fingertip, to detect slip. We obtained tactile sensor values corresponding to the slip and nonslip states in advance and created a training dataset with several patterns. Random Forest Classifiers were trained on the datasets, and the results were compared. All nine sensor elements in the sensor matrix could detect slips with practical accuracy in the real-time robot experiments. In time periods wherein no slip occurred, no nonslip states were erroneously determined as slip states under any of the tested conditions. The slip detector created in this study was demonstrated to be applicable to types of rope that were not used to train the detector.**

I. INTRODUCTION

Controlling flexible objects is a major challenge in robotic manipulation. This is because a flexible object can easily change shape, and control requires constant and appropriate feedback of the object's state. Slip state detection is especially important for controlling a flexible object because the robot manipulator must not apply more force than is needed to prevent the object from slipping. The slip of a grasped object can be detected by observing the change in the value of a load cell attached to the robot's arm. However, such sensors are expensive and cannot obtain information such as grasping position and orientation. Since humans can recognize the state of a grasped object based on their sense of touch, implementing tactile sensation in a robot's fingertips is one possible means to detect slip. Furthermore, if slip detection could be realized with a small and inexpensive tactile sensor, a low-cost and general-purpose system could be used to control the grasped object.

Ohkura et al. attached a sheet of a pressure sensor matrix to the finger of a robot and performed slip detection for a single rope [1]. However, their study assumed a specific rope and a specific hand movement, and the slip detection algorithm was designed ad hoc. In this study, we extend their previous work and propose a slip detection method under more general conditions. For this purpose, we consider appropriate fingertip shapes and materials and propose a learning-based slip detection algorithm.

[1]Takayuki Koga, Kohei Kimura and Shunsuke Kudoh are at the University of Electro-Communications, 5-1, Chofugaoka, 1-chome, Chofu-shi, Tokyo, Japan koga@robo.lab.uec.ac.jp, kimura@uec.ac.jp, s-kudoh@uec.ac.jp

[2]Junya Sato and Takuya Daigo are with Product Development Center at Japan Aviation Electronics Industry, Limited, 1-1, Musashino 3-chome, Akishima-shi, Tokyo 196-8555, Japan satoujn@jae.co.jp, daigot@jae.co.jp

The following studies have been conducted to classify slip and nonslip states of grasped objects. James et al. compared thresholding, linear, and nonlinear support vector machines (SVMs) and logistic regression (LR) using optical TacTip sensors [2]. Jiang et al. used a finger-skin inspired flexible optical (FIFO) sensor to detect strong spikes, which enables both force detection and slip detection [3]. Thomas et al. used a barometric tactile sensor and modeled the force distribution based on a bivariate normal Gaussian distribution. They detected slip with an average accuracy rate of 81.1% by applying threshold processing to the amount of movement of the grasped object [4]. David et al. used an ecological imitation optical tactile sensor based on human fingerprints to classify incipient slip and gross slip using SVM and Random Forest Classifier (RF). The accuracy rates of SVM and RF were 84% and 98%, respectively, for detecting the incipient slip in the validation data, which were similar in format to the training data. In the unlearned control, RF detected incipient slips were detected in the range of -418 ± 752 ms after the occurrence of the slip by using RF [5]. Some studies have compared several learning models. Euan et al. compared the accuracy of state classification by logistic regression (LR), SVM, RF, and long short-term memory (LSTM) using a soft force sensor with liquid metal. According to Euan et al., the RF model showed higher classification accuracy than the LSTM model that considered time series [6]. However, in many previous studies, the test object was a rigid object, the tests were conducted under a single condition, and numerous sensor elements were used. In this study, our objectives were to achieve slip detection of a rope with a robotic fingertip containing a tactile sensor matrix, and to verify that slip detection is applicable to various types of rope and modes of control.

Tactile sensors have been developed based on many different sensing principles. Optical sensors [7], [5] such as cameras can capture the deformation of flexible surfaces with high resolution [8]. However, while many optical tactile sensors can easily grasp the motion and shape of a grasped object, they often require excessive calibration. In magnetic tactile sensors [9], a permanent magnet is embedded in an elastic layer, and when a force acts on the sensor, the elastic layer deforms and displaces the magnet. Changes in the magnetic field caused by this movement are detected by a Hall sensor, and the contact force can be determined [10]. However, when handling objects that react to magnets, such as iron, the magnetic field changes, which makes it difficult to perform sensing. An advantage of barometric sensors [11], [12] is that, depending on the design of the sensor array, the actuation of one

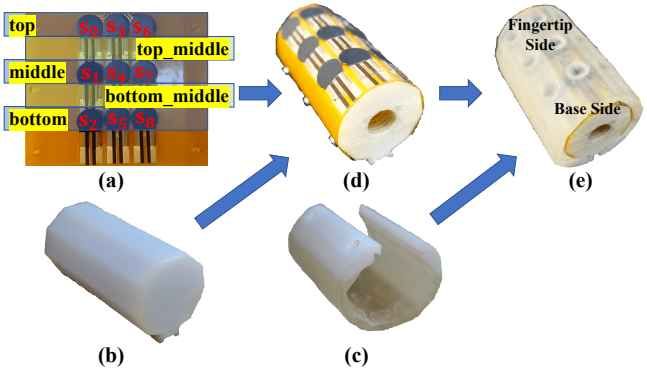

Fig. 1: Integration of tactile sensors into robot fingertip: (a)sensor sheet, (b)inner pillar, (c)outer grip, (d)sensor sheet with inner pillar, (e)Completed device.

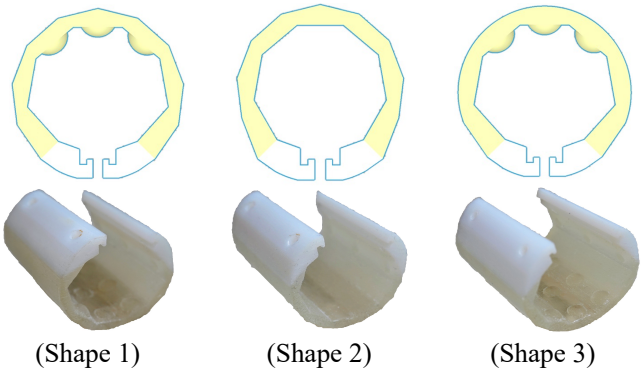

Fig. 2: Outer grip (Shape 1: 9-sided cylinder with protrusions, Shape 2: 9-sided cylinder without protrusions, Shape 3: R shape with protrusions).

sensor may enable other sensors to generate meaningful signals. However, a disadvantage of such sensors is that they saturate at low pressure levels (1 N) [13]. Piezoresistive tactile sensors serve well as dynamic sensors because of their large frequency response [14]. A common method for detecting slip using piezoresistive tactile sensors is to detect high-frequency vibrations that occur when slip occurs [13]. The amplitude of these vibrations increases as the sliding velocity increases [15]. Poly(vinylidene fluoride) (PVDF) is the most widely used piezoelectric polymer in artificial slip detection [16], and the frequency response of PVDF elements can be improved by placing fine bumps on the sensor surface [17]. From the above, piezoresistive tactile sensors are used for sensing in this study.

The main contribution of this study is to propose a method for detecting rope slips. For this purpose, we performed the following:

1) designing a method focusing on the stick-slip phenomenon, which is described later;
2) developing hardware by selecting the shape and material to easily capture stick-slip (described in Section IV. B.);
3) building an algorithm to detect stick-slip based on RF;
4) verifying the proposed method by conducting experiments with various types of rope and applying various kinds of force to them.

II. HARDWARE

The fingertip which was developed in this study consisted of sensor sheet, inner 9-sided cylinder and outer grip.

A. TACTILE SENSOR SHEET

To implement tactile sensation in a robot's fingertips, a tactile sensor sheet was created with pressure sensor elements (FSR400, sourced from Interlink Electronics) arranged in a 3×3 matrix as shown in Fig. 1(a). Each element is referred to as s_0 to s_8.

The dimensions of the sheet were 45 mm×53 mm. The positions of the sensor elements were the same as in Ohkura et al [1]. However, all sensor elements were glued to the FPC in this study, whereas Ohkura et al. did not completely fix the sensor elements to the FPC.

The pressure values applied to each element were obtained in 4096 steps from 0 to 4095 (0.8 mV/bit resolution) by A/D conversion and 12-bit conversion of the voltage from 0V to 3.3V, using Best Technology's DXMIO with an IMU. The sampling rate was set to 40 Hz, and the time stamps and sensor values of each element were obtained every 0.025 s.

As shown in Fig. 1(a), the grasping positions were divided into five patterns: 1) **top** overlapping with s0, s3, and s6; 2) **middle** overlapping with s1, s4, and s7; 3) **bottom** overlapping with s2, s5, and s8; 4) **top_middle** between the top and middle; 5) **bottom_middle** between middle and bottom.

B. INNER 9-SIDED CYLINDER

This inner pillar (Fig. 1(b)) consisted of a regular 9-sided cylinder with a side length of 7.875 mm, and a height of 45 mm. Using a prismatic shape made it easier to obtain tactile responses than when using a circular prism, because one row of the sensor matrix was able to be placed on a flat surface.

C. OUTER GRIP

To enhance the sensor's response, the sensor sheet was covered with elastomer grips. In the experiments described in the next section, three different hardnesses and three different shapes were tested. The three patterns of shapes shown in Fig. 2 were used in the experiments. Shore hardnesses A27, A60, and A95 were tested for Shape 1 and Shore hardness A27 for Shapes 2 and 3. A problem with the outer grip developed by Ohkura et al. was that the sensor element attached to the FPC was easily damaged when the inner pillar was inserted into the outer grip. Therefore, in this study, the upper part of the outer grip was detached and covered by the inner pillar. In addition, the ends of the grips were changed to hard elastomer in order to suppress the distortion of the grips caused by this change.

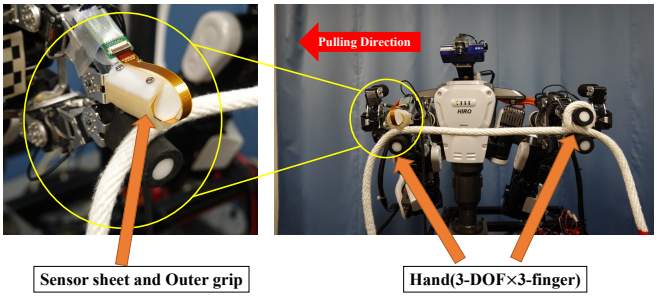

Fig. 3: The robot pulls the rope to the right hand direction.

III. DETERMINATION OF THE OUTER GRIP SHAPE AND HARDNESS

Experiments were conducted with dual-armed and multi-fingered robot to obtain datas, to determine the optimal shape and hardness.

A. Data Collection

An upper body humanoid robot, HIRO, manufactured by Kawada Industries, was used in the experiments. A servo operated 3-DOF×3-finger hand [18] was attached to each arm. The robot was allowed to grasp a rope, as shown in Fig. 3. The tactile sensor was attached to the upper finger of the right arm. One end of the rope was fastened to the left finger. Flexible objects such as ropes are stretched when tension is applied, making it difficult to capture changes in position and and the timing of slip with a camera or laser. Therefore, the state of the object was determined using values from the load cell (FFS055YA501U6 from Leptrino) attached to the robot's right arm.

The following back-and-forth motion was used in the experiment: the robot pulled the rope with a tension of F_c[N] for 5 s with right hand in the direction of the arrow (Fig. 3) and then shifted to the force-free state for 5 s (this was repeated four times). The force-free state is one in which the right arm exerts a very low tension (0.001 N) and the arm moves easily when a force is applied. Two different values of F_c (3 N and 9 N) were tested for each grip pattern in order to collect sensor values in the slip and nonslip states. The initial grasping position was set to the middle.

B. Data Analysis

A period from the time when tension started to the time when it ended was referred to as a "section."

1) Differences Depending on Hardness: Fig. 4 shows the graphs created from the experiments with the conditions of A27, Shape 1, and rope pulled at 9.0 N. Fig. 5 shows the graphs created from the experiments with the conditions of A95, Shape 1, and rope pulled at 9.0 N. In each graph, the horizontal axis shows the elapsed time, the blue line shows the sensor values, the red line shows the start time, and the orange line shows the slip start time. The tactile sensor values were obtained by subtracting the output value when the rope was grasped.

Vibration occurs when a slip occurs. This is a phenomenon called stick-slip described in [19], [20], according to which

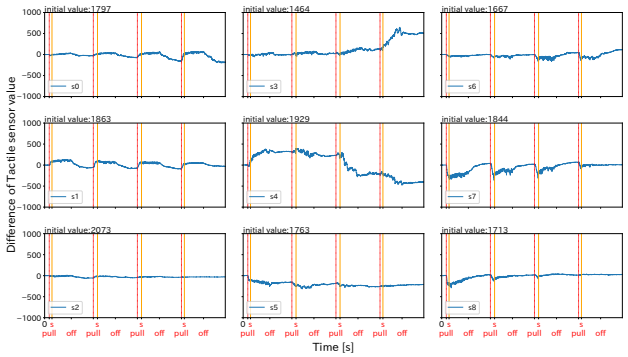

Fig. 4: Tactile sensor values (shore hardness: A27, shape: 9-sided cylinder with protrusions, target value: 9.0N).

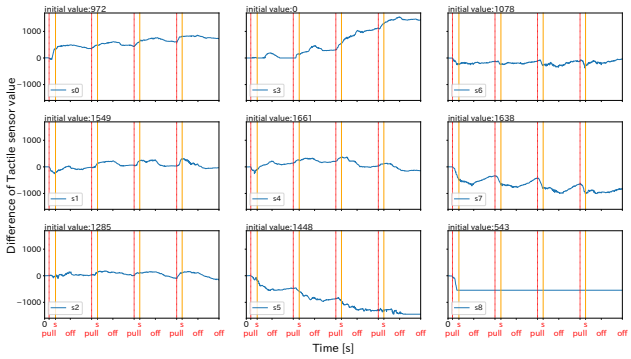

Fig. 5: Tactile sensor values (shore hardness: A95, shape: 9-sided cylinder with protrusions, target value: 9.0N).

the vibration is more likely to occur when the elasticity is high. Fig. 4 and Fig. 5 show that the oscillation of the sensor value decreased as the hardness increased, and the result is consistent with the theory. In this study, we apply this phenomenon to slip detection. Some studies have used this phenomenon as a signal of slip occurrence in slip detection using rigid materials [3], [6], [21]. It has also been suggested that similar properties can be observed in soft materials [19], [20]. As seen in Fig. 4, 5, there is increase in the sensor value on the s_3 side. This is likely due to the movement of the rope. Furthermore, in Figure 5, the curve for s_8 is a straight line without any fluctuations. This is thought to be due to a slight gap between the sensor element and the grip caused by deformation of the grip when force is applied.

2) Differences Depending on the Presence of Protrusions: The position of the center of gravity in terms of the x- and y-directions of the sensor value was obtained, according to the method given by Takahashi et al. [22]. Fig. 6 shows the trajectory of the center of gravity in the x-axis and y-axis every 150 steps. A number next to a red arrow in the figure is the time steps number. Due to the effect of the hand's torque, the rope gradually moved to the s_3 side. When tension was applied, the sensor value on the s_1 side increased. Each time tension was applied, the position of the center of gravity in the x direction became smaller and that in the y direction became larger, which is the actual change that is thought to be occurring. Therefore, comparing Fig. 6 (a) with (b), it can

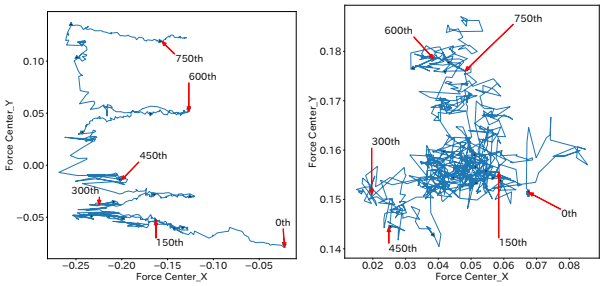

(a) Shore hardness: A27, shape: 9-sided cylinder with protrusions

(b) Shore hardness: A27, shape: 9-sided cylinder without protrusions

Fig. 6: The x-axis shows the center of gravity in the x-direction and the y-axis shows the center of gravity in the y-direction. The numbers next to red arrows indicate the time steps of that center-of-gravity position.

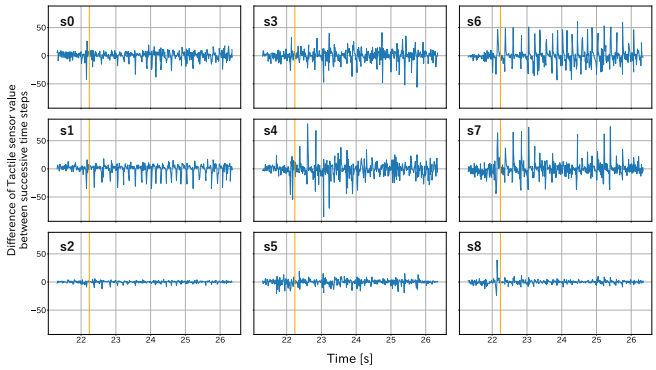

Fig. 7: Difference of tactile sensor values between successive time steps (Shore hardness: A27, shape: 9-sided cylinder with protrusions)

be said that the protrusions likely facilitate the detection of the grasping position.

3) Differences Depending on the Surface Shape: Fig. 7 and Fig. 8 present enlarged views of one control section and show the change in the force differences between successive datapoints. The 9-sided cylindrical grip yields large oscillations with a short period in the section where slip occurs, whereas the R-shaped grip yields large oscillations with a long period. It will be easier to detect continuous slip when large oscillations occur with a short period, so the 9-sided cylindrical grip is more suitable for slip detection. Table I shows the number of times that the value of s_1 was below -15 and the average value of s_1 when it was below -15 in Fig. 7 and Fig. 8.

Based on our findings thus far, we decided to use grips with Shore hardness A27, with protrusions, and with a 9-sided cylindrical surface in subsequent experiments.

TABLE I: The number of times that the value of s_1 was below -15 and the average value of s_1 when it was below -15 in Fig. 7 and Fig. 8

Fig. 7		Fig. 8	
Number of times	Average value	Number of times	Average value
29	-25.8	14	-57.3

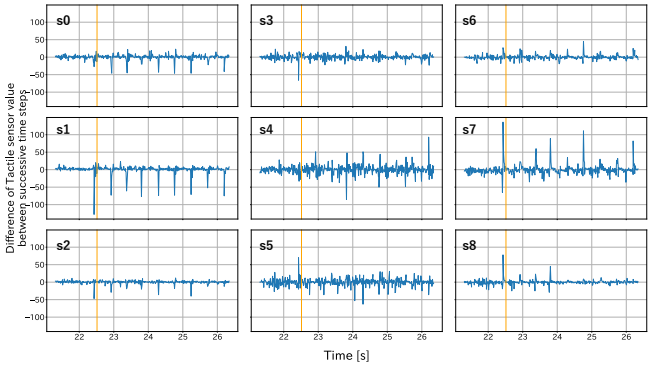

Fig. 8: Difference of tactile sensor values between successive time steps (Shore hardness: A27, shape: R shape with protrusions)

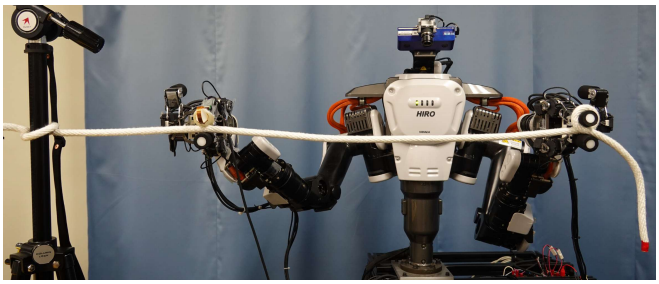

Fig. 9: The robot pulls the rope in the right-hand direction. The right end point of the rope is fastened.

IV. CREATING A SLIP DETECTOR

In this section, we describe a method for detecting slips from data obtained with tactile sensors. As a detection method, we use RF. First, we discuss the setting of the ground truth necessary for training, and then we describe the method of slip detection with RF.

A. Data Collection

As shown in Fig. 9, the measurement was taken with the right end point of the rope fastened to the post to prevent the rope from moving to the top or bottom side, and the left end point of the rope was fastened to the left fingers. Measurements were taken using two types of rope with different surface geometries (Fig. 10 (a), (c)), two modes of

Fig. 10: Types of rope: (a)12-strand vinylon rope, (b)12-strand nylon rope(12mm), (c)3-strand vinylon rope(12mm), (d)3-strand hemp rope(12mm), (e)12-strand nylon rope (7mm), (f)cable, and (e)PP tape.

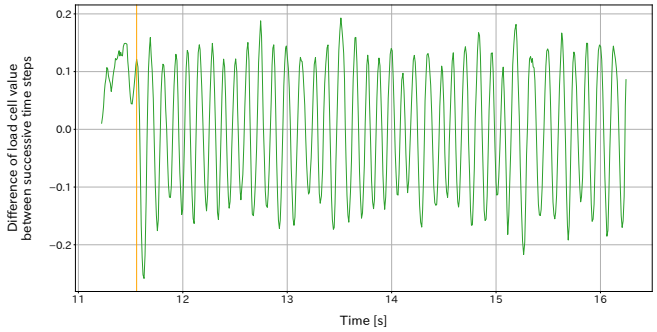

Fig. 11: Example of setting slip start time. The orange line indicates the slip start time.

control, and five grasping positions (Fig. 1 (a)). In addition, the grip selected in Section III were used. The two modes of control were force control and speed control:

Force Control

The robot pulled the rope with a force of f_1 and then with a force of f_2.

Speed Control

The robot pulled the rope at a velocity of v_1 and then at a velocity of v_2.

Each of the parameters is $(f_1, f_2) = (1, 3)$, $(5, 7)$, $(9, 11)$, $(13, 15)$, $(v_1, v_2) = (2, 4)$, $(6, 8)$, $(10, 15)$, $(20, 30)$. A total of 160 patterns (two types of rope $\times$ five grasping positions $\times$ two modes of control $\times$ eight parameters) were measured three times each. The tactile sensor values were sampled at 40Hz.

B. Ground Truth

As described above, we use the stick-slip phenomenon as a signal of slip occurrence in this study, and we attempt to detect this vibration by machine learning. For this purpose, a ground truth is necessary, and a load cell is used to set the ground truth, because it is easier to capture the vibration. This is because the tactile sensor has nine sensors, each of which produces different values depending on where the rope contacts. Therefore, using the load cell enables stable and accurate measurement of fingertip vibration. In this experiment, a load cell is attached to the robot and its data is recorded at the same time. Using this, the ground truth of the slip time is determined. Ground truth was set according to the following procedure.

- The difference between successive time steps for the load cell values was used (Fig. 11).
- The moving average of the values obtained in the previous procedure for the last five time steps was calculated and low-pass processing was applied.
- The time of the latest peak before the low-pass processed sensor value fell below the threshold, which was set to -0.02 in the experiment, was used as the slip start time.

C. Datasets for Training

In this study, slip was detected by machine learning using RF. In the previous study, RF had the best result among

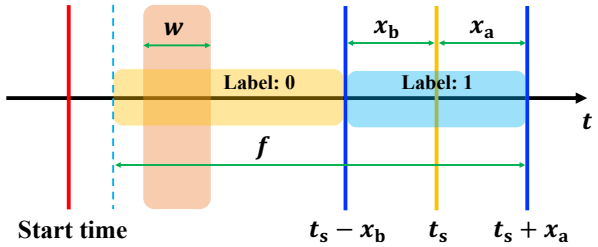

Fig. 12: Diagram of labeling.

TABLE II: Value of parameters and number of labels in each pattern

Pattern	w	f	$-x_b$ to x_a	Label: 0	Label: 1	Total
A	3	15	-0 to $+4$	4716	1773	6489
B	6	8	-0 to $+4$	2241	1773	4014
C	6	15	-4 to $+0$	4716	1773	6489
D	6	15	-2 to $+2$	4716	1773	6489
E	6	15	-0 to $+4$	4716	1773	6489

the machine learning methods [6]. Furthermore, RF is a robust model against the overfitting problem of traditional statistical methods that performs more efficiently for large-scale databases [23]. To create the dataset for training, the difference between the values of successive time steps was used instead of directly using the outputs from the sensors. Each observation used here was a $9w$-dimensional vector, which consists of the difference values from 9 sensors grouped by window width w. For each observation, RF was trained to return 1 if slip occurred within the corresponding window width, and 0 if slip did not occur.

The acquired data contained sections where slip occurred and sections where slip did not occur. In each case, the training dataset was created as follows.

1) Section where the slip occurred: The overview of dataset creation is shown in Fig. 12. Let t_s be the time when the slip occurred, which was obtained in the previous section. The range from x_b before to x_a after t_s was considered to be the range of slip occurrence. Observations overlapping with the range were labeled as 1, while the others were labeled as 0. To avoid an unbalanced number of positive and negative samples, only data from f time steps before $t_s + x_a$ were used.

2) Sections where no slip occurred: Twenty-five observations were generated from the start of each section and labeled as 0. The reason for the limited number of observations was to avoid an unbalanced number of positive and negative samples.

D. Results and Discussion

We created training datasets for several combinations of w, f, x_b, and x_a and compared the results after training. Table II shows the patterns that were tested.

The RF was trained using the Random Forest Classifier method of Python's sklearn library. The parameters of the RF were set to 400 for the *n_estimator* and to default values otherwise. The dataset was divided such that 90% of the dataset were used as training data and 10% as validation

TABLE III: Result of slip detection.

Pattern	Accuracy	Recall (non-slip)	Recall (slip)	Precision (non-slip)	Precision (slip)
A	91.3%	96.6%	77.2%	91.8%	89.4%
	97.6%	98.4%	80.0%	99.1%	69.9%
B	87.2%	87.6%	86.8%	89.3%	84.7%
	96.0%	96.0%	96.7%	99.9%	51.6%
C	81.4%	92.2%	52.8%	83.9%	71.3%
	96.2%	97.3%	71.7%	98.7%	54.4%
D	86.4%	95.4%	62.4%	87.1%	83.7%
	96.7%	97.7%	75.0%	98.9%	59.2%
E	91.3%	96.0%	78.7%	92.3%	88.1%
	98.1%	98.6%	87.5%	99.5%	73.4%

data. In addition, data from sections not used for training and validation data (32 sections) were used as test data.

Table III shows the results. The upper numbers are the results for the validation data, and the lower numbers are the results for the test data. Each indicator for the test data was calculated from the data from the start time to the end time for the section where no slip occurred and from the start time to $t_{\mathrm{s}} + x_{\mathrm{a}}$ for the section where slip occurred.

1) Differences depending on window size: Comparing Patterns A and E, we can see that the values of most indicators improved as window size increased. In particular, the recall of test data increased by 7%. This is likely because the larger window size made it easier to capture changes in sensor values and identify transitions from nonslip to slip states.

2) Differences depending on the amount of training data: Comparing Patterns B and E, Pattern E outperformed Pattern B in most indices. However, Pattern B has had a higher slip recall. This is thought to be because Pattern B had the same number of data points in the nonslip state as in the slip state. However, because the amount of learning required for the nonslip state was small, the precision for the nonslip state of Pattern B was low.

3) Differences depending on the position of the correct answer range: Comparing Patterns C, D, and E, when the correct answer range was placed after t_{s}, the values of all indicators were higher. This indicates that changes in sensor values before and after slip were captured appropriately. However, in Pattern C, the recall for slip was about 50%, which suggests that there were signs of slip before slip occurred.

Based on the above findings the parameters of Pattern E was used in the following experiments.

V. REAL-TIME ROBOT EXPERIMENT WITH SLIP DETECTION

The RF-based slip detector described in the previous section determines whether or not a slip has occurred for an observation at a certain point in time. In order to actually detect slips using this detector, it is necessary to detect slips repeatedly in real time while the robot manipulates the rope. In this section, we discuss such real-time slip detection.

TABLE IV: Result of real-time slip detection

Rope	Control mode	Number of errors (non-slip section)	$\overline{t_{\mathrm{p}} - t_{\mathrm{s}}}$ (time steps)	$\overline{t_{\mathrm{p}} - t_{\mathrm{s}}}$ [ms]
a	Force control	0	-7.0	-175.0
b	Force control	0	-12.7	-317.5
c	Force control	0	-0.67	-16.8
d	Force control	0	-4.67	-116.8
e	Force control	0	-0.33	-8.23
f	Force control	0	-0.33	-8.23
g	Force control	0	-0.67	-16.8
a	Speed control	-	0.0	0.0
b	Speed control	-	-4.50	-112.0
c	Speed control	-	-1.83	-45.8
d	Speed control	-	-1.33	-33.3
e	Speed control	-	-0.33	-8.3
f	Speed control	-	-0.33	-8.3
g	Speed control	-	-1.00	-25.0

A. Experimental setup

The experiment was conducted without fastening the right-hand end of the rope to the post, as shown in Fig. 3. Force control and speed control which were used in Section IV. A. were used to move the robot. Each parameter is $(f_1, f_2) = (4, 14)$, $(v_1, v_2) = (3, 13)$. For force control, parameters not used in Section IV.A were selected. The combination of selected parameters was the magnitude of force that would not absolutely cause slip and the magnitude of force that would absolutely cause slip. For speed control, we selected relatively small and large speeds that were not used in Section IV.A.

Seven types of ropes (Fig. 10 (a)$\sim$(g)) were used in the experiment. Each experiment was conducted three times and started from the middle position.

B. Results and Discussion

In practical use, even if a slip is not detected at the exact ground truth time, it is not a problem if a slip is detected at some other time around the ground truth. On the other hand, if a slip is detected even once when no slip has occurred, it should be considered as a misjudgment. In light of this, it is important to examine whether a slip is detected in a section where no slip has occurred, and how close to the ground truth t_{s} a slip is detected in a section where a slip has occurred. Table IV summarizes the experimental results based on the above. When speed control was conducted, there was no section where no slip occurred. The average difference in the time steps between t_{s} and the first time slip was detected in the section in which slip occurred was denoted by $\overline{t_{\mathrm{p}} - t_{\mathrm{s}}}$.

Table IV shows that there were no misjudgments in the nonslip section, and there were no slip sections where slips were not detected for any ropes. The mean and standard deviation for the entire experiment were -65.1 ms and 85.8 ms, respectively. This indicates that the proposed slip detector outputs slip timing much closer to ground truth than the detectors reported in previous studies [1], [5].

For the 12-strand rope (12mm), slip was detected much earlier than it occurred. The 12-strand rope had a large

elongation and stretched slightly when a force was applied, and early slip detection was inferred to be due to the weak vibrations that occurred during the application of force. In contrast, cable and PP tape had low elongation and high friction with grips. Therefore, we speculated that the vibration was larger, which facilitated slip detection.

Our findings indicated that slip could be detected for ropes that were not used for training with the same accuracy as for learned ropes.

VI. CONCLUSIONS

In this study, we proposed a method for detecting rope slips by using the vibration caused by the stick-slip phenomenon. First, we designed a fingertip with an embedded sensor sheet. The shape and hardness of the fingertip was determined by experimenting with different types of ropes. And then, the tactile sensor was integrated into a robot's fingertip. Tactile sensor values were collected in advance for different combinations of rope type, control mode, and grasping position when slip occurred and when slip did not occur. The detector was then created by training a RF classifier on the datasets and comparing the results. Based on the results of the experiment, the detection was successful with practical accuracy. However, several points are debatable. First, the vibration used for detection increases as the frictional force between the object and the grip increases, making it difficult to detect slips when the frictional force is small. Second, the accuracy of detection when using different robot motions from those in the experiment has not been verified. Third, as seen in Table III, when the number of labels in the data set is biased, the presicion value for the slip state becomes small. However, in this experiment, it is sufficient to correctly predict only one time step out of five time steps, so the effect of the small value of presicion on the slip state is considered to be small.

In this study, we considered the classification of nonslip state and the beginning of slip state, but we have not yet examined the predictive properties of continuous slip. In the future, we would like to make it possible to detect the states by training the proposed detector on these states as well. In addition, the current sensor structure and detector do not support the case in which there are multiple gripping points. By changing the shape of the grips and the arrangement and number of sensor elements, it may be possible to detect the state of each grasped object after detecting multiple gripping points.

REFERENCES

[1] Y. Okura, J. Sato, D. Takuya, M. Takizawa, S. Kudoh, and T. Suehiro, "Analysis of fingertip tactile sensors for slip detection of rope," in *SICE System Integration Division Annual Conference (SI)*, 2022, (in Japanese).

[2] J. W. James and N. F. Lepora, "Slip detection for grasp stabilization with a multifingered tactile robot hand," *IEEE Transactions on Robotics*, vol. 37, no. 2, pp. 506–519, 2021.

[3] C. Jiang, Z. Zhang, J. Pan, Y. Wang, L. Zhangand, and L. Tong, "Finger-skin-inspired flexible optical sensor for force sensing and slip detection in robotic grasping," *Advanced Materials Technologies*, vol. 6, 2021.

[4] T. D. Clercq, A. Sianov, and G. Crevecoeur, "A soft barometric tactile sensor to simultaneously localize contact and estimate normal force with validation to detect slip in a robotic gripper," in *2023 IEEE International Conference on Robotics and Automation (ICRA)*, 2023.

[5] D. C. Bulens, N. F. Lepora, S. J. Redmond, and B. Ward-Cherrier, "Incipient slip detection with a biomimetic skin morphology," in *2023 IEEE/RSJ International Conference on Intelligent Robots and Systems (IROS)*, 2023.

[6] E. Judd, B. Aksoy, K. M. Digumarti, H. Shea, and D. Floreano, "Slip anticipation for grasping deformable objects using a soft force sensor," in *2022 IEEE/RSJ International Conference on Intelligent Robots and Systems (IROS)*, 2022.

[7] Y. She, S. Wang, S. Dong, A. R. Neha Sunil, and E. Adelson, "Cable manipulation with a tactile-reactive gripper," *Robotics: Science and Systems XVI*, 2020.

[8] C. Trueeb, C. Sferrazza, and R. D'Andrea, "Towards vision-based robotic skins: a data-driven, multi-camera tactile sensor," in *2020 3rd IEEE International Conference on Soft Robotics (RoboSoft)*, 2020, pp. 333–338.

[9] Y. Yan, Z. Hu, Z. Yang, W. Yuan, C. Song, J. Pan, and Y. Shen, "Soft magnetic skin for super-resolution tactile sensing with force self-decoupling," *Science Robotics*, vol. 6, no. 51, 2021.

[10] C. Ledermann, S. Wirges, D.Oertel, M. Mende, and H. Woern, "Tactile sensor on a magnetic basis using novel 3d hall sensor-first prototypes and results," in *2013 IEEE 17th International Conference on Intelligent Engineering Systems (INES)*, 2013, pp. 55–60.

[11] J. W. Guggenheim, L. P. Jentoft, Y. Tenzer, and R. D. Howe, "Robust and inexpensive six-axis forcetorque sensors using mems barometers," *IEEE/ASME Transactions on Mechatronics*, vol. 22, no. 2, pp. 838–844, 2017.

[12] D. Mohtasham, G. Narayanan, B. Calli, and A. J. Spiers, "Haptic object parameter estimation during within-hand- manipulation with a simple robot gripper," in *2020 IEEE Haptics Symposium (HAPTICS)*, 2020, pp. 140–147.

[13] R. A. Romeo and L. Zollo, "Methods and sensors for slip detection in robotics: A survey," *IEEE Access*, vol. 8, 2020.

[14] R. S. Dahiya, G. Metta, M. Valle, and G. Sandini, "Tactile sensing-from humans to humanoids," *IEEE Trans. Robot.*, vol. 26, no. 1, pp. 1–20, 2010.

[15] I. Fujimoto, Y. Yamada, T. Morizono, Y. Umetani, and T. Maeno, "Development of artificial finger skin to detect incipient slip for realization of static friction sensation," in *Multisensor Fusion Integr. Intell. Syst. (MFI)*. IEEE Int, 2003, pp. 15–20.

[16] Y. Xin, H. Tian, C. Guo, X. Li, H. Sun, P. Wang, J. Lin, S. Wang, and C. Wang, "Pvdf tactile sensors for detecting contact force and slip: A review," *Ferroelectrics*, vol. 504, no. 1, pp. 31–45, 2016.

[17] Y. Yamada, H. Morita, and Y. Umetani, "A slip sensor with surface ridges which is mounted on a robot hand generates high-frequency signals for isolating slip phases," *The Society of Instrument and Control Engineers*, vol. 36, no. 6, 2000.

[18] M. Takizawa, S. Kudoh, and T. Suehiro, "Design and implementation of a multi-dof hand and basic motions for rope-knotting tasks," *Advanced Robotics (AR)*, vol. 36, no. 10, 2022. [Online]. Available: https://doi.org/10.1080/01691864.2022.2070866

[19] K. Nakano, "Conditional expression for the occurrence of stick-slip motion based on the coulomb friction model (part 1)," *Journal of Japanese Society of Tribologists*, vol. 51, no. 2, 2005.

[20] ——, "Conditional expression for the occurrence of stick-slip motion based on the coulomb friction model (part 2)," *Journal of Japanese Society of Tribologists*, vol. 51, no. 2, 2005.

[21] J.-K. Lee, H.-H. Kim, J.-W. Choi, K.-C. Lee, and S. Lee, "Development of direct-printed tactile sensors for gripper control through contact and slip detection," *International Journal of Control, Automation and Systems*, vol. 16, no. 2, pp. 929–936, 2018.

[22] H. Takahashi, J. Sato, T. Daigo, M. Takizawa, S. Kudoh, and T. Suehiro, "Rope sliding manipulation by using fingertip tactile sensor," in *SICE System Integration Division Annual Conference (SI)*, 2020, pp. 2546–2549, (in Japanese).

[23] M. Bagherian, E. Sabeti, K. Wang, M. A. Sartor, Z. Nikolovska-Coleska, and K. Najarian, "Machine learning approaches and databases for prediction of drug-target interaction: a survey paper," *Briefings in Bioinformatics*, vol. 1, no. 22, 2021.